Final Draft
of the original manuscript:

Hort, N.; Huang, Y.; Fechner, D.; Stoermer, M.; Blawert, C.; Witte, F.;
Vogt, C.; Druecker, H.; Willumeit, R.; Kainer, K.U.; Feyerabend, F.:
Magnesium alloys as implant materials – Principles of property design for Mg–RE alloys
In: Acta Biomaterialia (2009) Elsevier

DOI: 10.1016/j.actbio.2009.09.010

Magnesium Alloys as Implant Materials – Principles of Property Design for Mg-RE Alloys

N. Hort[a], Y. Huang[a], D. Fechner[a], M. Störmer[a], C. Blawert[a], F. Witte[b], C. Vogt[c], H. Drücker[c], R. Willumeit[a], K. U. Kainer[a], F. Feyerabend[a]

[a] GKSS Research Centre, Institute of Materials Research, Max-Planck-Str. 1, D-21502 Geesthacht, Germany

[b] Laboratory f. Biomechanics and Biomaterials, Hannover Medical School, Anna-von-Borries-Str.1-7, D-30625 Hannover, Germany

[c] Institute for Inorganic Chemistry, Leibniz University of Hanover, Callinstr. 9, D-30167 Hannover, Germany

Correspondence:

Dr. Norbert Hort, GKSS Research Centre, Institute of Materials Research, Magnesium Innovation Centre, Max-Planck-Str. 1, D-21502 Geesthacht, Germany

Phone: 0049 4152 87 1905, Fax: 0049 4152 87 1909

email: norbert.hort@gkss.de

Abstract

Magnesium alloys have gained increasing interest in the past years due to their potential as implant materials. This interest is based on the fact that magnesium and its alloys are degradable during their time of service in the human body. Moreover magnesium alloys offer a property profile that is very close or even similar to that of human bone. The chemical composition triggers the resulting microstructure and features of degradation. In addition the entire manufacturing route is having an

influence on the morphology of the microstructure after processing. Therefore composition and manufacturing route have to be chosen carefully with regard to the requirements of an application. This paper will discuss the influence of composition and heat treatments on microstructure, mechanical properties and corrosion behaviour of cast Mg-Gd alloys. Recommendations will be given for the design of future degradable magnesium based implant materials.

Keywords

Magnesium, rare earth elements, Gadolinium, mechanical properties, corrosion behaviour

1 Introduction

The increased interest in magnesium and its alloys as degradable material for implants led to numerous publications in this field [1-22]. Alloys like AZ91, AM50, LAE442, WE43 etc have been under investigation. Standard tests were applied and also mechanical properties and corrosion behaviour are evaluated under standard conditions and in simulated body fluids. From these tests the conclusion is drawn that these alloys are potential implant materials. This practice seems to be questionable to some extend due to the fact that in most cases the discussion is not considering all alloying elements and common impurities with regard to their interactions with cells.

In most cases standard commercial alloys contain more components than the designation is showing [23-29]. Almost any aluminium containing commercial magnesium alloy is also containing manganese in the range of 0.4-0.6 wt.-%. Even silicon is allowed in an amount up to 0.3 wt.-%. In general impurities may sum up to a total content of up to 0.3 wt.-% and very often these impurities are not listed in detail

or not even analysed. Moreover the composition is even more complicated when it comes to magnesium alloys that contain rare earth elements. The E in the designation of a number of magnesium alloys is representing rare earth elements (REE) in total (yttrium is having an own designation letter, W). In the standard practice of alloying Mg with REE so called hardeners are widely used. These are basically master alloys which contain a major REE like cerium or neodymium and almost any other REE in different amounts up to 25 wt.-% [29]. Especially when the alloy compositions are carefully contemplated it is obvious that in the case of REE containing magnesium alloys the influence of the entire group of REE is not thoroughly considered. In general in the case of standard alloys of the AZ, AM, WE and LAE series the impression is left that these materials have been simply selected because they are available.

For standard magnesium alloys the different alloying elements have been introduced for certain reasons. Due to the use of magnesium alloys as constructional materials quite often mechanical properties are standing in the first place of consideration. E. g. in the case of Al as alloying element it can be used both for solid solution strengthening and for precipitation hardening which are useful when the yield stress needs to be improved [24-30]. However, almost any strengthening is also having a detrimental influence on the ductility. With regard to the Mg-Al phase diagram it is also obvious that Al lowers melting and casting temperatures [31]. Therefore the use of Al has also an influence on the processing route. In consequence both the alloying elements and processing parameters are influencing the formation of the microstructure which is responsible for the application relevant properties. Similar considerations can be made for other alloying elements. .

Strength is often regarded as a critical property especially for a mechanical engineer. But it is not the only property that has to be considered [19, 28, 30]. Ductility, elastic moduli, corrosion behaviour under service conditions, rate of degradation (if applicable), toxicology amongst others are also part of the property profile which is basically influenced by the alloy composition and obviously by the different processing steps applied before a component is ready e.g. as a functional implant. The different properties that are required for an implant require also a vast number of different methods to determine them. This needs a highly interdisciplinary approach and interaction of specialists from different fields of research [19].

A number of cast Mg alloys containing gadolinium and additional REE have been investigated recently [32-52]. These investigations showed that Gd can be used to adjust mechanical properties in a wide range with regard to alloy composition and heat treatments due to its large solubility of 23.49 wt.-% at the eutectic temperature and the formation of intermetallic phases like Mg_5Gd (figure 1) [31]. As a single alloying element Gd is present in solid solution and it can be used in a concentration dependent manner to contribute to precipitation strengthening. Although many authors state that gadolinium is highly toxic, the acute toxicity is only moderate. The intraperitoneal LD_{50} dose of $GdCl_3$ was 550 mg/kg in mice **[53]** $GdNO_3$ induced acute toxicity in a concentration of 300 mg/kg (mice) and 230 mg/kg in rats, respectively [54]. Tests regarding the cytotoxicity of Gd on osteoblast like cells showed that it could be a suitable element to design Mg-Gd based implant materials for medical applications [55]. Additionally, evidence is rising that many rare earth elements exhibit anticarcinogenic properties, which could lead to multifunctionailty of the designated alloys [56-59]. On the other hand it is also known that Gd based contrast agents are

widely used in magnetic resonance imaging (MRI) as contrast media [60-62]. However, there are indications that Gd-ions released by transmetallation can induce nephrogenic systemic fibrosis in patients with renal failure, but not in healthy patients [63]. Despite that this would be a noteworthy problem in e.g. vascular applications Gd has also been observed to have a certain retention rate in bone prior to redistribution to spleen and liver [64]. With regard to this retention and the careful alloy design concerning the corrosion rate it can be envisaged that the release of Gd-ions could be controlled such that it would not evoke systemic effects. In this paper binary Mg-Gd alloys will be investigated to determine the influence of different amounts of Gd and of subsequent heat treatments on microstructure and properties.

2 Materials and Methods

For the present investigation Mg-2 wt.-%Gd, Mg-5 wt.-%Gd, Mg-10 wt.-%Gd and Mg-15 wt.-%Gd were used. High purity magnesium was molten in mild steel crucibles under protective atmosphere (Ar + 2 % SF_6). Gd was added as a pure element at a melt temperature of 750 °C. The melt then was stirred for 30 min with 200 rpm to avoid settling of Gd prior to casting. The melt was poured into preheated mild steel moulds (550 °C) to produce plates (300 mm x 210 mm x 30 mm) for further investigations. The mould is made up from two mirror inverted halves including the gating system. Figure 2 shows the schematic sketch of one half of the mould. To assure cleanliness of the cast ingots a filter (Foseco SIVEX FC) has been used.

All materials were investigated in the as-cast condition (F) and after solutionising (T4) and artificial ageing (T6) heat treatments [65]. For the T4 treatment a temperature of 525 °C was chosen and the specimens were annealed for 24 h. A water quench of the specimens followed immediately after the heat treatment. Ageing at 250 °C for

6 h was done for the T6 treatment on specimens that also have been solutionized for T4 conditions.

To investigate the microstructure all materials were grinded, polished and etched according to Kree et al. [66]. Microstructures were investigated using a Zeiss Ultra 55 (Carl Zeiss GmbH, Oberkochen, Germany) scanning electron microscope (SEM) including EDX to determine local chemical compositions. TEM investigations have been employed on thin foil samples of the different Mg-Gd alloys. The foils were prepared by electropolishing in a twin jet system using a solution of 2.5% $HClO_4$ and 95% methanol at -50°C and a voltage of 50 V. TEM examinations were carried out using a Philips EM20 instrument operating at 200 kV. For the analysis of the overall chemical composition ICP-OES has been employed (Spectroflame, Spectro, Kleve, Germany). The specimens have been dissolved in concentrated nitric acid and diluted by a factor of 32.000. Grain sizes have been determined using the line intercept method [67].

For the phase analysis X-ray diffraction (XRD) measurements were performed using a Bruker D8 Advance (Bruker AXS, Karlsruhe, Germany). The samples were investigated in parallel beam geometry, using Cu-Kα1 radiation (wavelength λ = 0.15406 nm). The X-ray diffractometer with a line focus is equipped with a Göbel mirror and a 1mm slit on the primary side. Because of the reflectometry stage of the diffractometer, the samples were aligned exactly at the goniometer centre. On the secondary side, there are a 0.6 mm backscattering slit and a 0.2 mm detector slit. The diffraction patterns were measured from 2 Θ (15–45°) for each sample. The increment was 0.04° and the step time was 64 s. For the qualitative phase identification of Mg_5Gd the PDF card #65-7133 from the International Centre for

Diffraction (ICDD) was used. The background of each diffraction pattern was subtracted and normalized to the maximum count rate of Mg (101).

Tension and compressive tests were performed for all conditions (F, T4, and T6) in accordance to DIN EN 10002 and DIN 50106 at room temperature using a Zwick 050 testing machine (Zwick GmbH & Co. KG, Ulm, Germany) [68, 69]. For the tension tests specimens with a gauge length of 25 mm and a diameter of 5 mm with threaded heads were used. The compression specimens had a length of 16.5 mm and a diameter of 11 mm. Elastic modulus E and the bulk modulus K have been calculated from the load-deformation curves using the testXpert® software package from Zwick.

The corrosion resistance of the alloys was investigated by immersion tests in standard eudiometer set-ups with a total volume of 400 ml and a resolution of 0.5 ml. The tests were performed in aerated 1% NaCl solution (starting pH 6.5, 21.5+/-0.5°C, without agitation). The specimens with dimensions of 11 mm x 11 mm x 11 mm were prepared by grinding each side with 1200 grid emery paper and degreasing the surfaces with ethanol prior to corrosion testing. The hydrogen evolution as an indicator of the corrosion rate was monitored after certain time periods. The average corrosion rate of each specimen at the end of the tests was calculated in mm/year by converting the total amount of collected hydrogen into material loss (1 ml H_2 gas = 0.001083 g dissolved Mg) and using the following equation (weight change Δg in g, surface area A in cm^2, time t in hours, density of the alloy ρ in g/cm^3):

$$CR = \frac{8.76 \cdot 10^4 \cdot \Delta g}{A \cdot t \cdot \rho}$$

This corrosion rate was cross checked by measuring the weight of the specimens before and after the corrosion test. The latter was done after cleaning and removal of

all corrosion products in chromic acid (180 g/l, 20 minutes immersion at room temperature).

Statistics were performed using the SigmaStat software package (Systat software GmbH, Erkrath, Germany). Standard analysis comparing more than two treatments was done by using the one-way ANOVA (all pairwise comparison). Depending on the data distribution either a one-way ANOVA or an ANOVA on ranks was performed. Post-hoc tests were Holm-Sidak or Tukey, respectively. Statistical values are indicated at the relevant experiments.

3 Results

3.1 Alloy Composition and Microstructure

The four alloys under investigations have nominal compositions of 2, 5, 10 and 15 wt.-% Gd,. In the alloys Mg2Gd, Mg5Gd, Mg10Gd, Mg15Gd is present in an amount of 1.87 ± 0.10 wt.-%, 4.67 ± 0.09 wt.-%, 9.20 ± 0.09 wt.-%, and 14.05 ± 0.10 wt.-%, respectively. The results are given after normalization to 100 %. For maximum precision of the results two different emission lines with negligible interferences have been used for the multifold measurements of each element. In all cases the real composition is around 8 % less compared to the nominal one.

The XRD measurements could not prove the presence of pure Gd, Mg_5Gd or oxides in the diffraction patterns for the alloys Mg2Gd, Mg5Gd and Mg10Gd. In these alloys only the typical Mg peaks are present. Mg_5Gd could be confirmed in the alloy Mg15Gd (figure 3, closed circles). The most intensive peaks of this structure are indexed, which are (333) and (660) in F and T6 condition. Mg_5Gd peaks can not be

observed in the T4 condition. The additional peaks (marked with closed squares) in the T6 condition are identified to belong to the metastable β' phase (figure 3).

The microstructures revealed by scanning electron microscopy are similar for all alloys. Differences exist only in the amount of precipitates. Precipitates resembling the Mg_5Gd phase were found in all alloys. Figure 4a shows a typical SEM graph of the microstructure of the Mg15Gd alloy in the as cast state (F). It is obvious that particles of different morphologies are present. For their identification EDX analysis was performed on these particles. Typical particles are shown in figure. 4b-d. An EDX investigation in the matrix also brought the result that the average oxygen content is in the range of 0.5 at.-%.

In figure 4b the white particle 1 is chosen as an example for the first type of particles. It is extremely rich in Gd (83.5 at-.%) and contains additionally some Mg (13.4 at.-%) and O (3.1 at.-%). It shows a very regular blocky shape. Grey particles like particle 2 can be found very often (figure 4c). The EDX analysis of this particle indicates that it is rich in Mg (86.3 at.-%) and Gd (12.7 at.-%). It also contains some O (1.0 at.-%). In the microstructure additional small particles like particle 3 were found which are rich in Mg, Gd (figure 4d). Both elements are present at almost the same level. Moreover an amount of more than 12 at.-% oxygen is present in particle 3.

The eutectic phase Mg_5Gd can be observed at grain boundaries in all as-cast samples. These particles have a size in the micrometer range (figure 5a). After T4 treatments most of these particles dissolve but some still remain (figure 5b). The subsequent T6 treatment leads to the precipitation of very fine particles in a nanometer scale (figures 6a and 7a) in all alloys exept for Mg2Gd. The selected area diffractions (figures 6b and 7c) indicate that these fine precipitates are the metastable

phases β' and β'' after ageing. The β' phase is homogeneously distributed over the matrix (figure 7a and b). β'' can only be observed in limited areas. It has a crystal structure that is similar to those of Mg. β'' is completely coherent with the matrix of magnesium alloy. The lattice parameter a of β' is twice that of Mg. β' has a c-based centred orthorhombic structure (a = 0.641 nm, b = 2.223 nm, c = 0.521 nm).

In the as-cast Mg-Gd alloys, the grain size decreases with increasing the content of Gd (figure 8). After solutionising or T6 treatments the grain size increases especially for the alloys with less than 10 wt.-%Gd. However, for the alloy with 15 wt.-% Gd, the grain is really stable during heat treatments.

3.2 Mechanical Properties

Figure 9 presents the mechanical properties obtained in tension and compression tests. It is almost obvious that an increasing amount of Gd improves the ultimate tensile strength (UTS) as well as the tensile yield strength (TYS) while at the same time the elongation to fracture (El) is reduced. In the F condition and in the T6 condition TYS, UTS and El are almost similar for the alloy Mg2Gd while in T4 a reduction of TYS, UTS and El can be observed. However, the differences are not significant (all statistical values and significance level are summarized in table x). Mg5Gd in general is showing higher TYS and UTS and a similar El compared to Mg2Gd. Mg5Gd is having the highest values for TYS and UTS in the as cast condition. The following heat treatments (T4, T6) are resulting in a significant decrease of TYS and UTS. El is only significantly decreased in the T6 state. Mg10Gd is showing a behaviour that is almost comparable to Mg2Gd in the trend. In the T4 state TYS and UTS are significantly reduced. Differences in the values for elongation were not significant. But as mentioned before, the increasing amount of Gd improves

strength but reduces ductility when both alloys are compared. Mg15Gd is presenting the highest values for the TYS and the UTS but also the smallest ductility El. The T6 treatment led to significant increases in TYS and UTS.

Like in tension a similar trend can be observed in compression tests as well regarding the amount of alloying elements. An increase of Gd leads to an increase of compressive yield strength (CYS), ultimate compressive strength and a decrease of the deformation in compression (Compr). For Mg2Gd the T4 and T6 heat treatments are not changing the UCS significantly. The CYS is significantly lowered by the T4 treatment and can be increased again during the T6 treatment to a significantly higher level than in the F state. The deformation in compression can be regarded as similar for all conditions. Mg5Gd is having slightly better values for CYS, UCS and also for the deformation in compression. The UCS is significantly lowered in the T4 and T6 condition, while the decrease of te CYS is only significant in the T6 treated condition. Mg10Gd follows the trend with increasing values for CYS and UCS compared to the previous alloys. The T4 treated specimens is lowering CYS and UCS significantly, the T6 treatment can reveal these properties to values that are comparable to the F condition. It is also interesting to see that the deformation in compression is almost comparable in every state. Mg15Gd shows the highest CYS and UCS values compared to the other alloys. Like before the T4 treatment leads to a significant decrease of CYS and UCS and is slightly improving the deformation in compression. Maximum values are obtained in the T6 treated Mg15Gd but to the expenses of a highly significant reduced deformation in compression.

For the bulk modulus K the heat treatments exhibited no significant influences. However, increasing the amount of Gd leads to an increase in K. K is 33.3 ± 9.1 GPa,

38.7 ± 8.1 GPa, 41.0 ± 5.7 GPa, 42.5 ± 3.4 GPa for Mg2Gd, Mg5Gd, Mg10Gd, Mg15Gd, respectively. Significant differences were determined by ANOVA for Mg10Gd (Mg10Gd vs. Mg2Gd: $t=2.970$, $p<0.005$) and Mg15Gd (Mg15Gd vs. Mg2Gd: $t=3.536$, $p<0.001$). This is not observed for the Young's modulus. E is 39.1 ± 10.4 GPa, 39.9 ± 4.1 GPa, 43.6 ± 3.2 GPa, 41.1 ± 10.3 GPa for Mg2Gd, Mg5Gd, Mg10Gd, Mg15Gd, respectively and no significant differences between the alloys as well as the different conditions could be determined (ANOVA). Within the error the values for E have to be regarded more or less the same despite different amounts of Gd in the four alloys.

3.3 Corrosion Behaviour

The corrosion rates (CR) were determined by calculations based on the hydrogen formation and the weight loss. Figure 10 shows the corrosion behaviour of the Mg-Gd alloys in the F condition. With increasing amounts of Gd up to 10 wt.-% the corrosion rate is decreased. Higher Gd values like in the alloy Mg15Gd lead to a drastic increase in the corrosion rate.

4 Discussion

4.1 Alloy composition and Microstructure

The analysis of the Gd content showed that the real compositions are generally a lower content compared to the nominal composition. A loss of 10 % of REE during melting and casting was already reported [24]. This loss of alloying elements is a well known phenomenon and is called "melting loss" [70]. As reported in the experimental section the melt was stirred after adding the Gd. Moreover a melt temperature of more than 700 °C has to be regarded as critical for the protective gas SF_6 because

its efficiency is reduced at these temperatures [29]. Due to interactions of alloying elements with the environment and components of the protective gases a certain amount of Gd can react. This leads to the formation of an oxide Gd_2O_3 which has a higher density (7.41 g cm^{-3}) compared to the Mg alloy melt (1.54 g cm^{-3}) [25]. During casting the used filter can remove these oxides. But due to the fact that the filter is still relatively coarse some particles like oxides or even pure remaining alloying elements can be transported into the castings (figure 4b and c).

With respect to principles of solidification and the chosen compositions only the phase Mg_5Gd can form [30, 31, 70]. During solidification the concentration of Gd in the solid is in accordance to the concentration at the solidus line at a given temperature and in equilibrium with the concentration in the melt at the liquidus line. The material solidifies completely latest at the eutectic temperature of 548 °C. The solidified material is also cooling down slowly and allows precipitation of Mg_5Gd. Therefore in all alloys some amount of Mg_5Gd exists. With regard to the fact that with increasing temperature the α matrix is showing an increasing solubility, all T4 conditions for all alloys should be free from Mg_5Gd and additionally precipitates can form again due to the T6 treatment.

Pure Gd or Mg_5Gd phases could not be proven by the XRD measurements for the alloys Mg2Gd, Mg5Gd and Mg10Gd. Moreover the measurements show that oxides are also not present. The Mg_5Gd phase has been verified by XRD in the Mg15Gd alloy in condition F and T6 (closed circles, figure 3). Additionally all Mg peaks (open diamonds) are shifted towards lower angles which indicate that some of the Gd atoms are still solved in the Mg matrix.

In condition T6 additional peaks appeared between 17-25° (marked with closed squares, figure 3) and have been identified as peaks of the metastable Mg-Gd β' phase. Like in other Mg-RE alloys such as Mg-Y-x alloys (where x is Nd, Ce or Gd), the precipitation sequence in Mg-Gd alloys can be given as [79-81]:

β'' -> β' -> Mg_5Gd

β'' and β' phases were observed by TEM in the aged Mg-15Gd alloy (figures 6 and 7). The final equilibrium phase Mg_5Gd was not observed under the present ageing conditions. The present ageing temperature and time cannot meet the requirement by the precipitation of this phase from the view of thermodynamics and kinetics. In WE alloys the formation of equilibrium phase Mg_5Gd need more than 2000 hours when they were aged at 250°C [79]. This indicates that it is difficult to precipitate the equilibrium phase Mg_5Gd. Vostry et al. also reported that the precipitates are mainly β' phase in Mg15Gd alloy when it was aged less than 25 hours [80]. They further indicated that the metastable β' phase is responsible for the peak hardening in Mg-Gd alloys. The present Mg15Gd alloy with T6 treatment was aged at 250°C only for 6 hours. Consequently, only the metastable phase β' (with little β'' phase) can be observed in the aged Mg15Gd alloy. There is no evidence of β'' because its amount is below the threshold level for the detection by XRD.

With respect to the fact that intermetallic phases consisting of Mg and Gd have been observed in all alloys in the metallographic investigations the XRD measurements can be explained in a way that the amount of intermetallic phases or oxides for the alloys with less than 15 wt.-% Gd is below the detection threshold level of 1-2 % [71, 72]. But with regard to the fact that a fairly large amount of precipitates can be seen this explanation is not fully satisfying.

The Cu-Kα1 radiation can also be used to explain that Mg_5Gd and even other phases like oxides could not be detected. The energies of the L edges of Gd are below those of Cu leading to fluorescence. Therefore the background is relatively high and peaks of phases may be covered. The ration of peak intensity to the background in is the range of 1:4. The strong background as well as the interaction of Gd and the Cu-Kα1 radiation is leading to a small penetration depth in the range of 2 µm while this is in Mg normally in the range of around 100 µm. This definitely reduces the volume that is available for analysis and lowers the possibility to detect phases that could be observed in microscopy. Additionally the unit cell of Mg_5Gd is relatively large and consists of 72 atoms. The amount of unit cells contributes directly to the intensity of the peaks and the large number of Gd in a single unit cell allows therefore only a limited number of unit cells. This reduces the intensity of the reflexes and can explain the weak intensity even of the strongest peaks of Mg_5Gd.

EDX measurements show the presence of Mg, Gd and O in all analyzed particles. The electron beam used for the analysis interacts not only with the surface that is investigated but also with the bulk material to a depth of a few microns [73]. A scatter has not been determined due to the uncertainty of the composition in the electron beam interaction volume. In the case of Mg and an acceleration voltage of 15 keV the penetration depth is in the range of a few microns. In general the particles are to small and in almost any case the matrix in the electron interaction volume is influencing the measurement. Therefore a certain amount of Mg in the particles detected by EDX measurements is coming from the matrix itself.

In figure 4b a particle is shown that contains mainly Gd (83.5 at.-%), some Mg (13.4 at.-%) and O (3.1 at.-%). The Mg content is assumed to originate from the bulk

material which is also having a typical content of O in the range of 0.5 at.-%. In particle 1 the O content is significantly higher compared to the matrix. When the melt was prepared it was stirred after addition of Gd and additionally the melt temperature was adjusted to 750 °C. SF_6 is not fully efficient at this melt temperature. This allows oxygen to come into contact with the melt and alloying elements. Gd is also showing a higher affinity to oxygen rather than Mg [50, 74]. Therefore Gd oxides can form. This may either be in the form of Gd_2O_3 or as a spinell $MgGd_2O_4$. This gives an indication that perhaps the surface of this particle is covered with an oxide layer. This layer can act as a diffusion barrier and prevents further oxidation. Mg is having less affinity to oxygen compared to most rare earth elements and is therefore not able to break the oxide layer.

The analysis of the grain size showed that the grains in all alloys and under all conditions are fairly coarse. The reason is a relatively slow cooling rate during casting due to the high melt temperature, a high mould temperature (550 °C) and a thickness of 30 mm of the cast plate. This results in a negligible undercooling and therefore in a small amount of nuclei only. An increasing amount of Gd decreases the grain size for all F conditions. This effect is also well known [24, 75-78]. In general alloying elements contribute to grain refinement to some extend and also Gd is doing so.

The T4 heat treatment results in an increase of grain size in all cases except the Mg15Gd. Due to the relatively high temperatures for solutionising, most of the Mg_5Gd intermetallics at grain boundaries in the alloys Mg2Gd, Mg5Gd, and Mg10Gd are dissolved and the grains can grow. It can be stated that within the error these three alloys reach almost a similar grain size of 700-800 µm.

A grain growth can even be observed in the T6 treated conditions for Mg5Gd. For Mg2Gd and Mg10Gd the values remain comparable to those in the T4 conditions. The grain growth during T6 treatment for Mg5Gd is caused by the T4 solution treatment.

The grain size for the alloy Mg15Gd remains stable during the different heat treatment regimes. The reasons are stable Mg_5Gd intermetallic phases and oxides on the grain boundaries which are pinning them. This explanation is in agreement with the literature [29, 52, 79].

4.2 Mechanical properties

The increase in strength (TYS and UTS) with increasing amounts of Gd is mainly attributed to the increase of Gd in solid solution in the α matrix. The difference is significant when TYS and UTS of Mg15Gd are compared to the alloys with equal or less than 10 wt.-% of Gd. As expected an increase in strength is not improving the elongation to fracture. To some extent the formation of intermetallic phases that have been formed during solidification or in respect of the heat treatments is also contributing to this effect. Due to the solutionising temperature of 525 °C and the solutionising time of 24 h almost any precipitates of Mg_5Gd are dissolved during the T4 treatments. Additionally for the alloys with Gd contents equal or less than 10 wt.-% a grain growth also could be observed. Both the dissolution of precipitates as well as the grain growth contributes to the loss in strength that could be observed after the T4 treatments.

The elongation stays almost at the same level for Mg2Gd and Mg5Gd but is improved in the alloys with 10 and 15 wt.-% Gd. Due to the higher amount of Gd in

the alloys Mg10Gd and Mg15Gd there are more β' intermetallics present at the grain boundaries. When they disappear the alloys get more ductile. But still the annealing time of 24 h at a temperature of 525 °C is not sufficient to dissolve all precipitates in the alloy Mg15Gd. The grain size is still stable and TYS as well as UTS are at comparable level to the F condition for the alloy Mg15Gd.

The results regarding compressive yield strength (CYS), ultimate compressive strength (UCS) and the compressive deformation (Compr) follow a similar trend compared to the results obtained in tension. The major difference lies in the fact that the absolute values are higher compare to the results from tensile tests. The difference is based in the fact that porosity exists in the alloys and is acting different under tension or compression. While pores are opened in tension and will lead to early failures this is not the case in compression. Here the pores are closed and are not really affecting the testing method itself. This results generally in higher absolute values for CYS, UCS and compressive deformation.

A comparison of the different alloy compositions and the different conditions of the materials also show that the tensile yield stress can be varied between 33 MPa and 200 MPa. The lowest UTS is 78 MPa and the highest is reaching 250 MPa. The elongation to fraction is at a minimum at a value of around 1 % while it reaches a maximum at 6 %. With regard to the coarse microstructure where the grain sizes are larger than 350 µm the elongations to fracture can be regarded as very attractive. Using grain refining agents or an increase of the cooling rates would result in a much finer grains structure. With regard to the fact that in general a finer grain is improving strength without deteriorating ductility a further improvement of the tensile properties can be expected in further development of the alloys.

The reason for this behaviour is the different mode of loading in tension and compression. While porosity is affecting tension properties negatively and as well the calculation of the elastic modulus this is not the fact in compression. Under compression all pores will be closed first and will not lead to initial cracks and crack propagation. In fact pores are present in all castings [70]. Due to shrinkage during solidification and that feeding is not possible in all cases under standard solidification conditions microporosity is present.

K is increasing with the increasing amount of alloying elements. The differences between the alloys are significant. In contrast to K the statistical analysis of E shows no significant differences between the alloys. In general this has to be interpreted in a way that tensile tests can not be regarded as really reliable methods to determine these values. Similar observations have been reported frequently since more than 60 years especially for the Young's modulus of magnesium and its alloys [24-27, 82]. Due to these observations it seems that E is not really constant. The Young's modulus is susceptible to the applied load, composition, internal stresses that occurred during manufacturing, and processing etc. In difference to these limitations of E it has not been reported that the Young's modulus of magnesium alloys is affected by heat treatments. As a conclusion it has to be said that especially the uncertainty in the determination of Young's modulus of magnesium and its alloys deserves additional effort in research to solve this problem in future.

4.3 Corrosion Behaviour

Both the determination of corrosion rates by eudiometer tests and weight loss gain in almost similar results. Therefore both methods have to be regarded as suitable and can be directly compared. Slight differences for Mg15Gd might be due to not

complete removal of all corrosion products in the cleaning process and some not considered variations of temperature and pressure which influence the determination of the amount of hydrogen.

With an increasing amount of Gd up to 10 wt.-% the corrosion behaviour is improved. This finding is also in agreement with investigations of Rokhlin [52]. For 15 wt.-% Gd a drastic increase in the corrosion rate is observed. Contrary to the other binary alloys Mg15Gd has the smallest grain size. This also means that compared to the other binary alloys the fraction of grain boundaries is larger. Moreover the phase Mg_5Gd can be found mainly on grain boundaries and has to be regarded as more noble compared to the matrix [83]. As a third observation the Ni content in the Mg15Gd is the highest that could be observed.

4.4 Recommendations for orthopaedic applications

All properties of the implant material and the implant design have to be chosen in relation to its use in the musculo-sceletal or the cardiovascular system of the human body. The selection of a suitable application has to be made first.

As a second step it is necessary to evaluate the biological environment. Magnesium alloys can be absorbed by the human body. It is indispensable that the released elements are non-toxic, especially in the case of degradable materials [19, 22, 55]. It is strictly recommended to determine the impact of the release of alloying elements on human cells or on cell lines in *in vitro* tests which are accepted within standard tests [19, 21, 55]. It already could be shown that standard tests like the MTT assay are not completely suitable [84]. As a further recommendation standard test have to be checked if they can be safely applied on magnesium alloys and the products that are

set free or created during degradation. *In vivo* studies have to be performed, as at present no real correlation between *in vitro* and *in vivo* results can be deducted [2, 19].The knowledge on the efficiency of alloying elements regarding toxicology leads to list of elements that can be used for alloy design.

The implant material has to achieve certain degradation behaviour, strength under tension, compression, bending and torsion as well as fatigue values to assure the proper mechanical behaviour as well as to avoid e.g. stress shielding as much as possible when a material is used as a bone implant. All these factors are basically based on the microstructure. Microstructure formation is due to alloying elements and processing parameters. As a next step it is therefore recommended to select alloying elements in combination with a processing route that produces materials with a property profile that is as close to the bone in the area of application.

The selection of an application and the required properties is giving the frame for the design of implants. This is followed by alloying and the selection of appropriate processing to obtain a microstructure which determines the property profile in a first approach. As long as the target requirements are not reached alloy and process development in combination with testing the property profile, *in vitro* and *in vivo* behaviour needs to be repeated until the target requirements are reached.

5 Summary

The binary alloys analysed in this study are designated to be used as bone implants. The tensile strength of cortical bone is related to the species, age, anatomical location and testing conditions. In general the property profile of the Mg-Gd alloys under investigation is much closer to the values of cortical bone and their elongation

to fracture is even better compared to other metallic implant materials like stainless steels, titanium alloys and cobalt-chromium alloys. Furthermore the TYS, UTS, CYS and UCS of the investigated Mg-Gd can be adjusted over a wide range which makes them promising candidates for the future design of degradable metallic implants.

Gd is a suitable alloying element for the design of magnesium implant alloys. Due to the large solubility of Gd in Mg it contributes to solid solution strengthening. Larger levels of Gd above 10 wt.-% additionally improve strength due to precipitation hardening. The increasing solubility of Gd with increasing temperature makes the system Mg-Gd also very attractive to heat treatments to adjust the mechanical properties in accordance to the requirements of the property profile of an application as a medical implant. With regard to different concentration of Gd and heat treatments the mechanical properties and corrosion behaviour of these Mg-Gd alloys can be varied in a wide range. Tensile yield stress can be adjusted within 33-200 MPa, ultimate tensile strength within 79-250 MPa. This equals a variation of 600 % for the TYS and 300 % for the UTS, respectively. Minimum compressive yield strength is 38 MPa, the maximum reaches 216 MPa. The ultimate compressive strength is in the range of 157-395 MPa. The variation in the CYS stress is at 550 % and for the UCS 250 %, respectively. The extremely wide ranges in mechanical properties will allow the use of these alloys in applications where the requirements may be completely diverse.

6 Acknowledgements

The authors want to express their acknowledgement to V. Kree, S. Schubert, G. Meister and W. Punessen for their technical support.

7 References

1 Krause C et al., Mechanical properties of degradable magnesium implants in dependence of the implantation duration, Magnesium Technology in the Global Age, Pekguleryuz M. O, Mackenzie L. W. F, editors, 2007;329-343

2 Witte F, Kaese V, Haferkamp H, Switzer E, Meyer-Lindenberg A, Wirth CJ, Windhagen H, In vivo corrosion of four magnesium alloys and the associated bone response, Biomaterials 2005; 26 ;3557-3563

3 Witte F. et al., Cartilage repair on magnesium scaffolds used as a subchondral bone replacement, Materialwissenschaft und Werkstofftechnik 2006; 37;504 – 508

4 Witte F. et al., Magnesium- hydroxylapatite composite: A novel approach to degradable biomaterials, Biomaterials 2007; 28 ;2163-2174

5 Witte F, Ulrich H, Rudert M, Willbold E, Biodegradable magnesium scaffolds: Part 1: Appropriate inflammatory response, Journal of Biomedical Materials Research 2007; 81A ;748-756

6 Witte F, Ulrich H, Palm C, Willbold E, Biodegradable magnesium scaffolds: Part II: Peri-implant bone remodeling, Journal of Biomedical Materials Research 2007;81A;757-765

7 Kuwahara H et al., Surface reaction of magnesium in Hank´s solution, Materials Science Forum 2000; 350-351;349-58

8 Erbel R et al., Temporary scaffolding of coronary arteries with bioabsorbable magnesium stents: a prospective, nonrandomised multicentre trial, Lancet 2007; 369;1869-75

9 Heublein B, Rohde R, Kaese V, Niemeyer M, Hartung W, Haverich A,

Biocorrosion of magnesium alloys: a new principle in cardiovascular implant technology?, Heart 2003; 89;651-56

10 Witte F, Fischer J, Nellesen J, Crostack HA, Beckmann F, Windhagen H, Synchrotron-radiation based microtomography for in-vivo corrosion measurements of magnesium alloys, ORS Transactions 2006; 31;937

11 Witte F et al., In vitro and in vivo corrosion measurements of magnesium alloys, Biomaterials 2006; 27;1013-1018

12 Witte F, Fischer J, Nellesen J, Beckmann F, Microtomography of Magnesium Implants in Bone and their Degradation, SPIE Proc: Developments in X-Ray Tomography, San Diego, USA, 13.-17.08.2006, 631806

13 Waksman R et al., Safety and efficacy of bioabsorbable stents in procine coronary arteries, Catheterization and Cardiovascular Interventions 2007; 68;607-617

14 Zhang GD, Huang JJ, Yang K, Zhang BC, Ai HJ, Experimental study of in vivo implantation of a magnesium alloy at early stage, Acta Metallurgica Sinica 2007; 43;1186-1190

15 Xu LP, Yu GN, Zhang E, Pan F, In vivo corrosion behavior of Mg-Mn-Zn alloy for bone implant application, J. Biomedical Materials Research A 2007;83;703-711

16 Feyerabend F, Witte F, Kammal M, Willumeit R, Unphysiologically high magnesium concentrations support chondrocyte proliferation and redifferentiation, Tissue Eng. 2006; 12;3545-3556

17 Kaya RA, Cavusoglu H, Tanik C, Kaya AA, The effects of magnesium particles in posterolateral spinal fusion: an; experimental in vivo study in a sheep model,

J. Neurosurgery-Spine 20072; 6;141-149

18 Zartner P, Cesnjevar R, Singer H, Weyand M, First successful implantation of a biodegradable metal stent into the left pulmonary artery of a preterm baby, Catheter Cardiovasc Interv 2005; 66;590-594

19 Witte F, Hort N, Vogt C, Cohen S, Kainer KU, Willumeit R, Feyerabend F, Degradable Biomaterials based on Magnesium Corrosion, Current Opinion in Solid State and Materials Science 2008:12:63-72

20 Witte F, Abeln I, Switzer E, Kaese V, Meyer-Lindenberg A, Windhagen H, Evaluation of the skin sensitizing potential of biodegradable magnesium alloys, Journal of Biomedical Materials Research Part A 2008; 86;1041-1047

21 Feyerabend F, Hort N, Witte F, Kainer KU, Willumeit R, In vitro corrosion and cytocompatibility of two magnesium alloys, Regenerative Medicine 2007;2;612

22 Drynda A, Deinet N, Braun N, Peuster M, Rare earth metals used in biodegradable magnesium-based stents do not interfere with proliferation of smooth muscle cells but do induce the upregulation of inflammatory genes, Journal of Biomedical Materials Research Part A, in press

23 ASTM B951-07, Standard Practice for Codification of Unalloyed Magnesium and Magnesium-Alloys, Cast and Wrought, doi: 10.1520/B0951-08

24 Emley EF, Principles of Magnesium Technology, Pergamon Press, New York, USA, 1966

25 Kammer C, Magnesium Taschenbuch, Aluminium Verlag, Düsseldorf, Germany, 2000

26 Beck A, The Technology of Magnesium and its Alloys, F. A. Hughes & Co. Ltd, London, UK, 1940

27 Raynor GV, The Physical Metallurgy of Magnesium and its Alloys, Pergamon Press, New York, USA, 1959

28 Avedesian MM, Baker H, ASM Specialty Handbook: Magnesium and Magnesium Alloys, Materials Park, OH: ASM International, 1999

29 Friedrich HE, Mordike BL, Magnesium Technology – Metallurgy, Design Data, Applications, Springer, Berlin, Germany, 2006

30 Callister WD, Materials Science and Engineering, John Wiley & Sons Inc, Hoboken, NJ, USA, 7th edition, 2006

31 Nayeb-Hashemi AA, Phase Diagrams of Binary Magnesium Alloys, ASM International, Metals Park, Ohio, USA, 1998

32 Peng Q, Wang J, Wu Y, Wang L, Microstructures and tensile properties of Mg-8Gd-0.6Zr-xNd-yA (x+y = 3, mass%) alloys, Materials Science and Engineering A 2006; 433;133-138

33 Apps PJ, Karimzadeh H, King JF, Lorimer GW, Phase composition in magnesium-rare earth alloys containing yttrium, gadolinium or dysprosium, Scripta Materialia 2003;48; 475-481

34 Apps PJ, Karimzadeh H, King JF, Lorimer GW, Precipitation reactions in Magnesium-rare earth alloys containing Yttrium, Gadolinium or Dysprosium, Scripta Materialia 2003;48;1023-1028

35 Chang J, Guo X, He S, Fu P, Peng L, Ding W, Investigation of the corrosion for Mg–xGd–3Y–0.4Zr (x = 6,8, 10,12 wt%) alloys in a peak-aged condition, Corrosion 2008;50;166-177

36 Cizek J, Prochazka I, Smola B, Stulikova I, Ocenasek V, Influence of deformation on precipitation process in Mg–15 wt.%Gd alloy, Journal of Alloys

and Compounds 2007;430;92–96

37 Gao L, Chen R.S, Han E.H, Effects of rare-earth elements Gd and Y on the solid solution strengthening of Mg alloys, Journal of Alloys and Compounds 2009, in press, doi:10.1016/j.jallcom.2009.02.131

38 Gao X, He S M, Zeng X Q, Teng L M, Ding WJ, Nie JF, Microstructure evolution in a Mg-15Gd-0.5Zr (wt.%) alloy during isothermal aging at 250 °C, Materials Science and Engineering A 2006;431;322-327

39 Gao Y, Wang Q, Gu J, Zhao Y, Tong Y, Behavior of Mg–15Gd–5Y–0.5Zr alloy during solution heat treatment from 500 to 540 ◦C, Materials Science and Engineering A 2007;459;117–123

40 Guo Y, Li J, Li J, Yang Z, Zhao J, Xia F, Liang M, Mg–Gd–Y system phase diagram calculation and experimental clarification, Journal of Alloys and Compounds 2008;450;446–451

41 He SM, Zeng XQ, Peng LM, Gao X, Nie JF, Ding WJ, Microstructure and strengthening mechanism of high strength Mg–10Gd–2Y–0.5Zr alloy, Journal of Alloys and Compounds 2007;427;316–323

42 Honma T, Ohkubo T, Hono K, Kamado S, Chemistry of nanoscale precipitates in Mg-2.1Gd-0.6Y-0.2Zr (at.%) alloy investigated by the atom probe technique, Materials Science and Engineering A 395 2005;395;301-306

43 Kulyasova OB, Islamgaliev RK, Kil'mametov AR, Valiev RZ, Superplastic Behavior of Magnesium-Based Mg–10 wt % Gd Alloy after Severe Plastic Deformation by Torsion, The Physics of Metals and Metallography, 2006;101;585–590

44 Liu K, Zhang J, Rokhlin LL, Elkin FM, Tang D, Meng J, Microstructures and

mechanical properties of extruded Mg–8Gd–0.4Zr alloys containing Zn, Materials Science and Engineering A 2009;505;13–19

45 Peng Q, Wang L, Wu Y, Wang L, Structure stability and strengthening mechanism of die-cast Mg–Gd–Dy based alloy, Journal of Alloys and Compounds 2009:469;587–592

46 Peng Q, Hou X, Wang L, Wu Y, Cao Z, Wang L, Microstructure and mechanical properties of high performance Mg–Gd based alloys, Materials and Design 2009;30;292–296

47 Peng Q, Dong H, Wang L, Wu Y, Wang L, Aging behavior and mechanical properties of Mg–Gd–Ho alloys, Materials Characterization 2008;59;983-986

48 Peng Q, Dong H, Wu Y, Wang L, Age hardening and mechanical properties of Mg–Gd–Er alloy Journal of Alloys and Compounds 2008;456;395–399

49 Peng Q, Wu Y, Fang D, Meng J, Wang L, Microstructures and Properties of Melt- Spun and As- Cast Mg-20Gd Binary Alloy, Journal of Rare Earths 2006;24;466 470

50 Wang X, Wu W, Tang Y, Zeng X, Yao S, Early high temperature oxidation behaviors of Mg–10Gd–3Y alloys, Journal of Alloys and Compounds 2009;474;499–504

51 Gröbner J, Schmid-Fetzer R, Selection of promising quaternary candidates from Mg-Mn-(Sc, Gd, Y, Zr) for development of creep-resistant magnesium alloys, Journal of Alloys and compounds 2001; 320;296-301

52 Rokhlin LL, Magnesium alloys containing rare earth elements – Structure and properties, Taylor & Francis, London, UK, 2003

53 Haley TJ, Raymond K, Komesu N, Upham HC, Toxicological and

pharmacological effects of gadolinium and samarium chlorides, Br J Pharmacol Chemother 1961;17: 526-32

54 Bruce DW, Hietbrink BE, DuBois KP. The acute mammalian toxicity of rare earth nitrates and oxides. Toxicology and Applied Pharmacology 1963;5:750-759

55 Feyerabend F et al., Evaluation of short term effects of rare earth and other elements used in magnesium alloys on primary cells and cell lines, Acta Biomaterialia, submitted

56 Dai Y, Li J, Yu L, Dai G, Hu A, Yuan L, Wen Z, Effects of rare earth compounds on growth and apoptosis of leukemic cell lines, In Vitro Cell Dev Biol Anim 2002; 38;373-375

57 Ji Y, Li J, Xiao B, Wang ZH, Cui MZ, Lu YY, The suppression effect of light rare earth elements on proliferation of two cancer cell lines, Biomed Environ Sci 2000; 13;287-292

58 Kostova I, Momekov G, Stancheva P, New Samarium(III), Gadolinium(III), and Dysprosium(III) Complexes of Coumarin-3-Carboxylic Acid as Antiproliferative Agents, Met Based Drugs (2007) 15925

59 Magda D, Miller RA, Motexafin gadolinium: A novel redox active drug for cancer therapy,Seminars in Cancer Biology 2006; 16;466-476

60 Heinrich MC et al., Cytotoxicity of iodinated and gadolinium-based contrast agents in renal tubular cells at angiographic concentrations: In Vitro Study, Radiology 2006; 242;425-434

61 Thomsen HS, Gadolinium-based contrast media may be nephrotoxic even at approved doses, Eur Radiol 2004;14;1654-6

62 Maiseyeu A et al., Gadolinium containing phosphatidylserine liposomes for molecular imaging of atherosclerosis, J. Lipid Res. (2008) M800405-JLR200

63 ten Dam MA, Wetzels JF, Toxicity of contrast media: an update. Neth J Med 2008;66:416-422

64 Wedeking P, Kumar K, Tweedle MF. Dose-dependent biodistribution of [^{153}Gd]Gd(acetate)n in mice. Nuclear Medicine and Biology 1993;20:679-691

65 ASTM B296, Standard Practice for Temper Designations of Magnesium Alloys, Cast and Wrought, doi:10.1520/B0296-03R08

66 Kree V, Bohlen J, Letzig D, Kainer KU, The metallographical examination of magnesium alloys, Practical Metallography 2004;41;233 – 246

67 ASTM E112, Standard test methods for determining average grain size, doi:10.1520/E0112-96R04E02

68 DIN EN ISO 10002, Tension testing of metallic materials, Beuth Verlag, Berlin, Germany, 2001

69 DIN 50106, Compression testing of metallic materials, Beuth Verlag, Berlin, Germany, 1978

70 Campbell J, Castings, Butterworth Heinemann, Oxford, UK, 2nd edition, 2003

71 Jenkins R, Snyder RL, Introduction to X-ray powder diffractometry, J. Wiley & Sons, New York, USA, 1996

72 Snyder RL, X-ray diffraction, in: Lifshin E, editor, X-ray characterisation of Materials, Wiley-VCH, Weinheim, Germany, 1999;1-103

73 Potts PJ, A Handbook of Silicate Rock Analysis, Springer, Berlin, Germany, 1987

74 ASM Metals Handbook, Desk Edition, 2nd edition, ASM International, Metals

Park, Ohio, USA, 1998

75 Lee YC, Grain refinement of Magnesium, PhD Thesis, University of Queensland, Australia, 2002

76 Cao P et al., Native grain refinement of magnesium alloys, Scripta Materialia 2005: 53:841-844

77 Lee YC et al., The role of solute in grain refinement of magnesium, Metallurgical and Materials Transactions A 2000; 31;2895-2906

78 StJohn DH, Qian M, Easton MA, Cao P, Hildebrand Z, Grain Refinement of magnesium alloys, Metallurgical and Material Transactions A 2005; 36;1669-1679

79 Nie J F, Muddle BC, Characterization of Strengthening Precipitate Phases in a Mg-Y-Nd Alloy, Acta Mater. 2000; 48;1691-1703

80 Vostry P, Smola B, Stulikova I, von Buch F, Mordike BL. Microstructure evolution in isochronally heat treated Mg-Gd alloys. Phys Status Solidi A 1999;175:491.

81 Yang Z, Li JP, Guo YC, Liu T, Xia F, Zeng ZW, Liang MX. Precipitation process and effect on mechanical properties of Mg-9Gd-3Y-0.6Zn-0.5Zr alloy. Mat Sci Eng 2007;454:274.

82 S. Kleiner, Thixocasting, Textur und mechanische Anisotropie von stranggepressten Magnesiumlegierungen, Dissertation, ETH Zürich, Zürich, CH, ETH Nr. 15013, 2003

83 Song GL, Atrens A, Corrosion mechanisms of magnesium alloys, Advanced Engineering Materials 1999;1:11-33

84 Fischer J, Prosenc M, Wolff M, Hort N, Willumeit R, Feyerabend F, Tetrazolium

Salt - based Assays are not suitable for Cytotoxicity Testing of Magnesium and its Alloys, Acta Biomaterialia, submitted

Figures

Figure 1: Mg-Gd phase diagram

Figure 2: Schematic sketch of the mould geometry (one half)

Figure 3: XRD patterns of Mg15Gd alloys (closed circles: fcc Mg_5Gd phase, open diamonds: pure hcp Mg, closed squares: orthorombic β'

Figure 4: a) SEM micrograph of the alloy Mg15Gd in condition F, b) particle 1 consists mainly of Gd (rectangular shape, white), c) Mg5Gd (grey) particle 2, d) particle 3 is rich in Mg, Gd, and O

Figure 5: Morphologies of second phases Mg_5Gd. (a) large particles Mg_5Gd in as-cast Mg-15Gd alloy, (b) remaining particle after heat treated at 525°C for 24h. The diffraction zone is [255]

Figure 6: (a) Morphology of β'' phase; (b) the corresponding diffraction pattern, the strong spots belongs to Mg and weak spots to β'' phase. It shows the β'' phase has a complete coherent relationship with Mg matrix. The diffraction zone is [110].

Figure 7: (a) Morphology of β' phase at low magnification; (b) Morphology of β' phase at high magnification; (c) The corresponding diffraction rings.

Figure 8: Grain sizes of the Mg-Gd alloys in the different heat treated conditions

Figure 9: Mechanical Properties of the Mg-Gd alloys in tension a) F, b) T4, c) T6 and in compression d) F, e) T4, f) T6

Figure 10: Corrosion rates determined by hydrogen generation and weight loss measurements

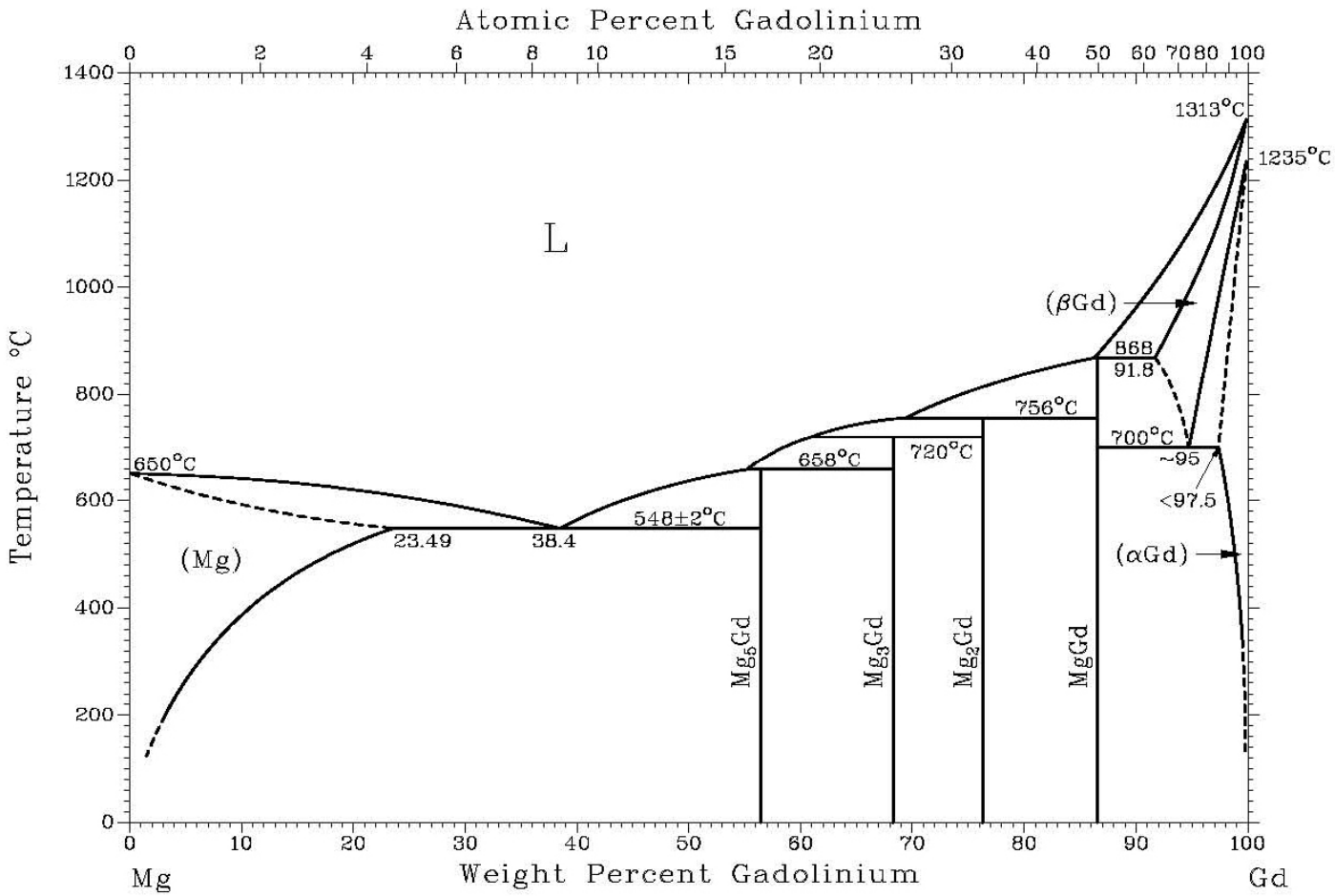

Figure 1: Mg-Gd phase diagram /31/

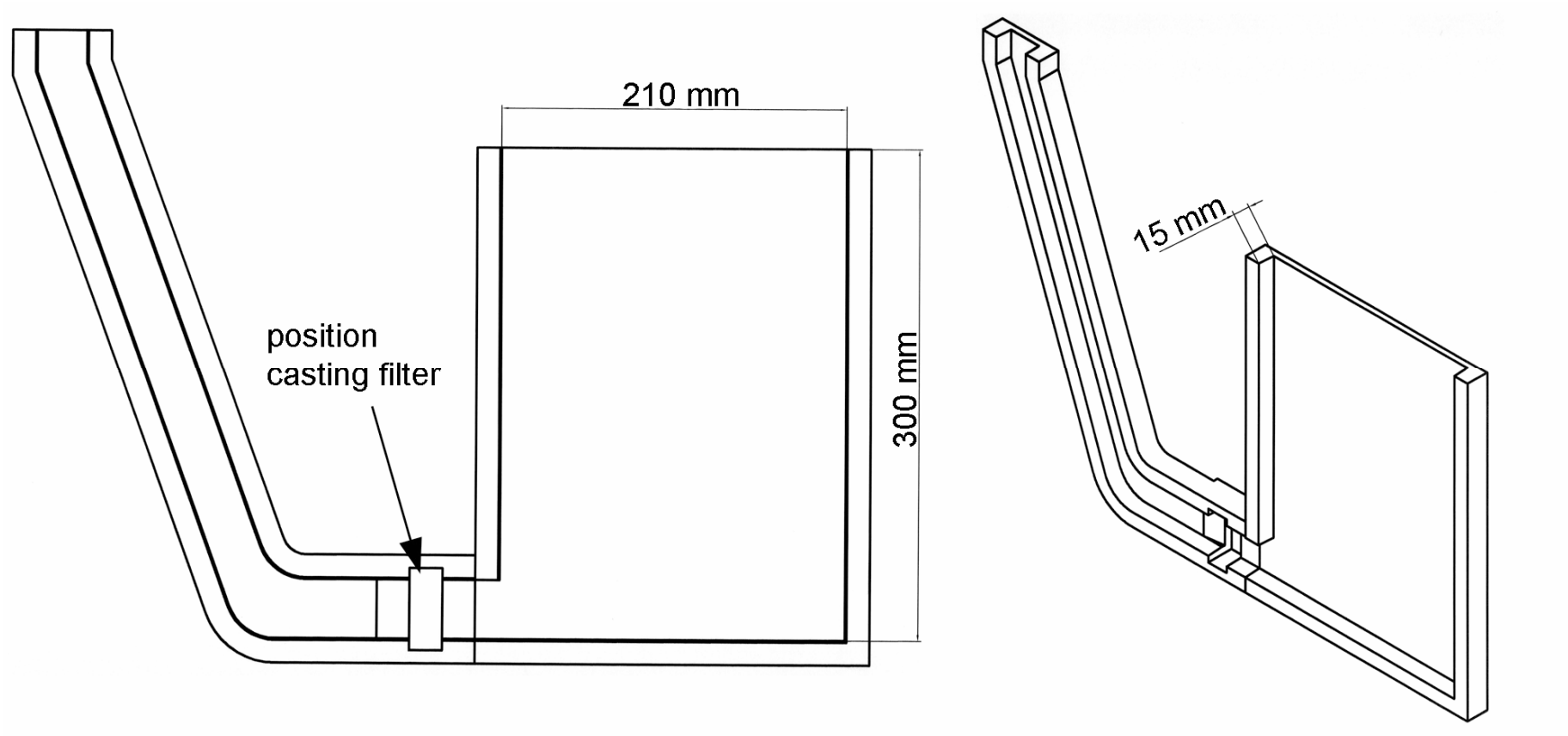

Figure 2: Schematic sketch of the mould geometry (one half)

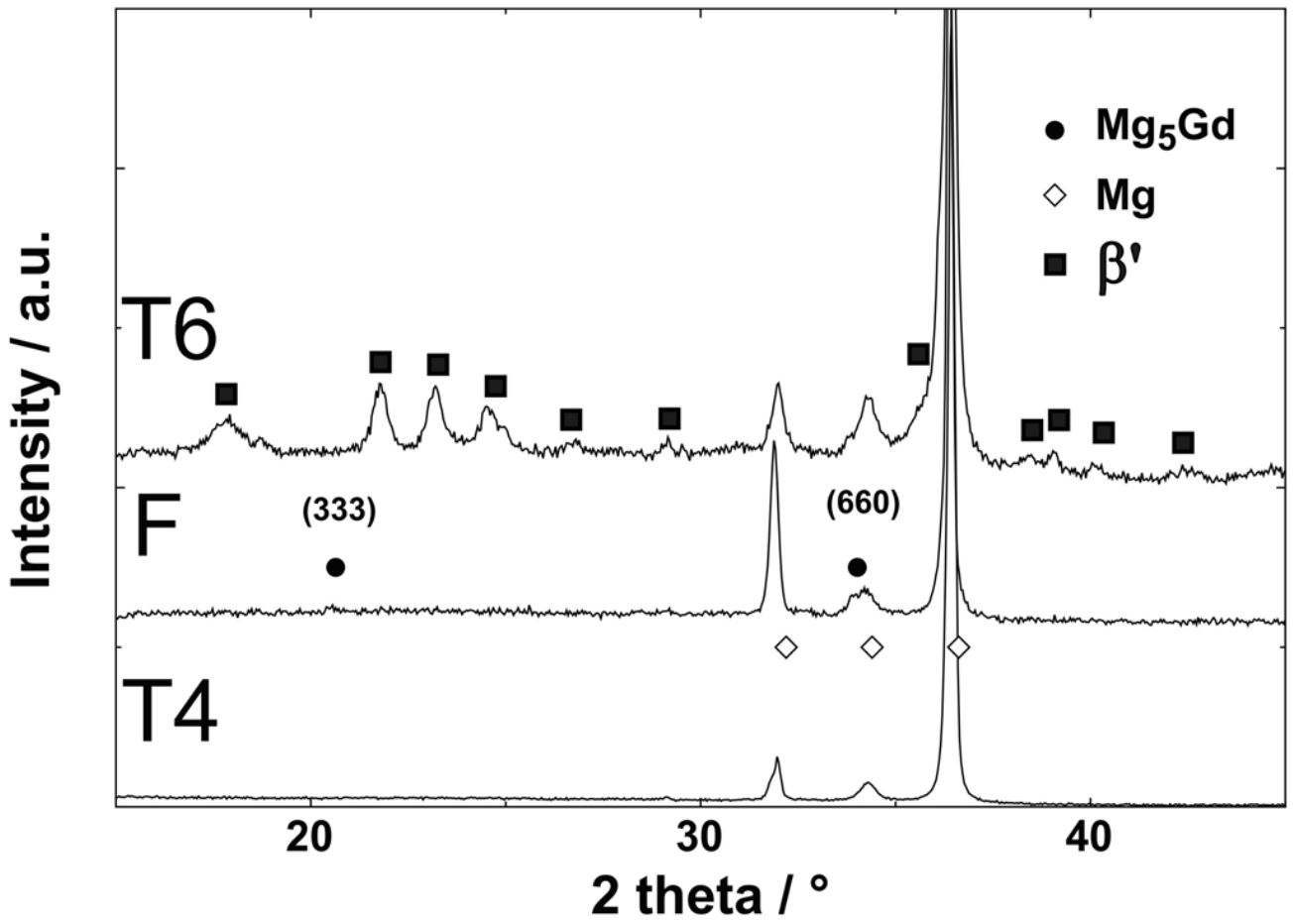

Figure 3: XRD patterns of Mg15Gd alloys (closed circles: fcc Mg_5Gd phase, open diamonds: pure hcp Mg, closed squares: orthorombic β'

a)

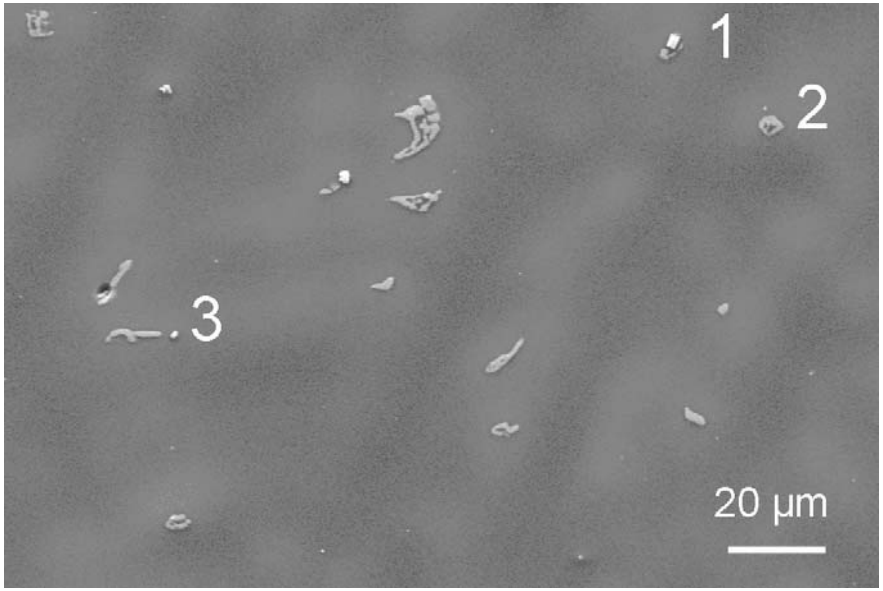

b)

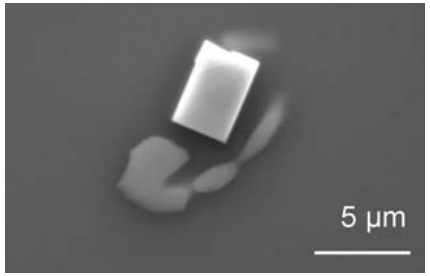

c)

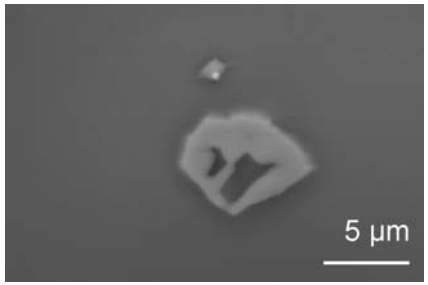

d)

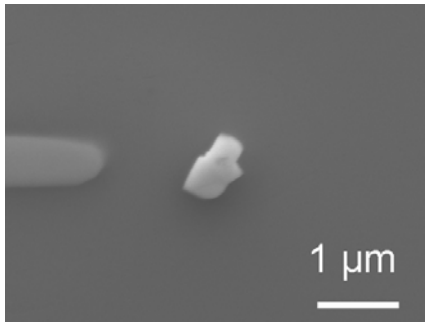

Figure 4: a) SEM micrograph of the alloy Mg15Gd in condition F, b) particle 1 consists mainly of Gd (rectangular shape, white), c) Mg5Gd (grey) particle 2, d) particle 3 is rich in Mg, Gd, and O

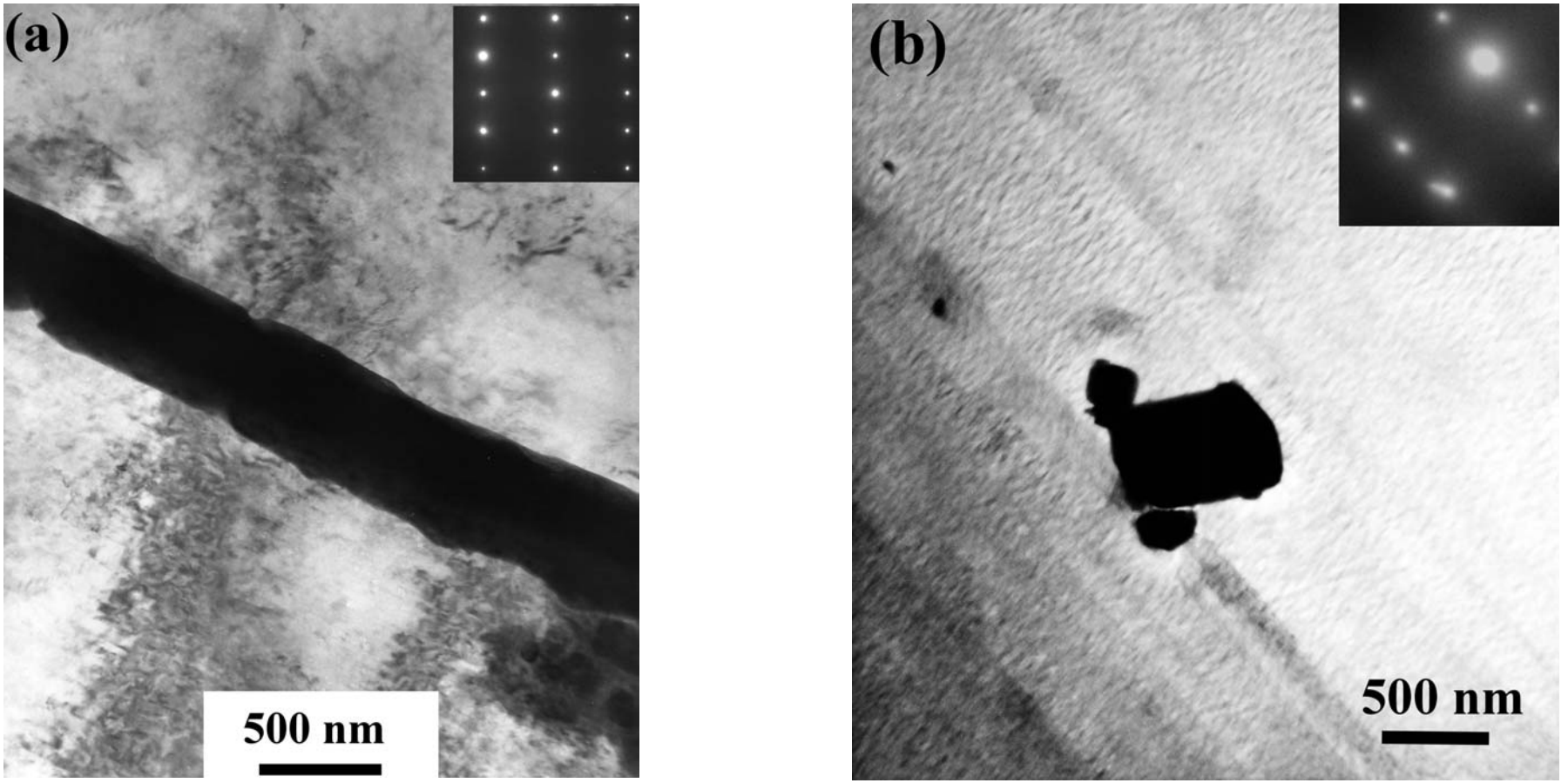

Figure 5: Morphologies of second phases Mg_5Gd. (a) large particles Mg_5Gd in as-cast Mg-15Gd alloy, (b) remaining particle after heat treated at 525°C for 24h. The diffraction zone is [255]

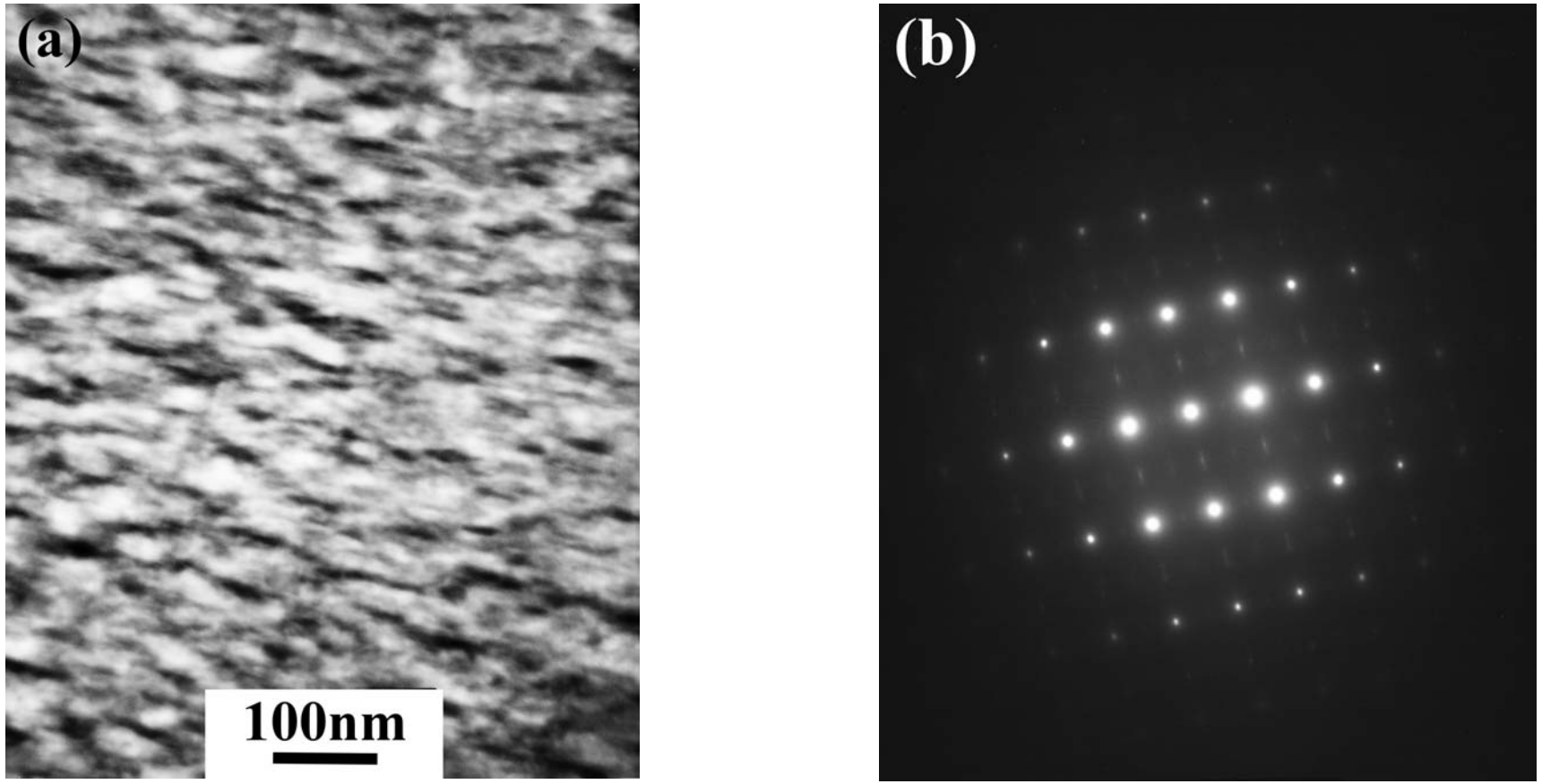

Figure 6: (a) Morphology of β'' phase; (b) the corresponding diffraction pattern, the strong spots belongs to Mg and weak spots to β'' phase. It shows the β'' phase has a complete coherent relationship with Mg matrix. The diffraction zone is [110].

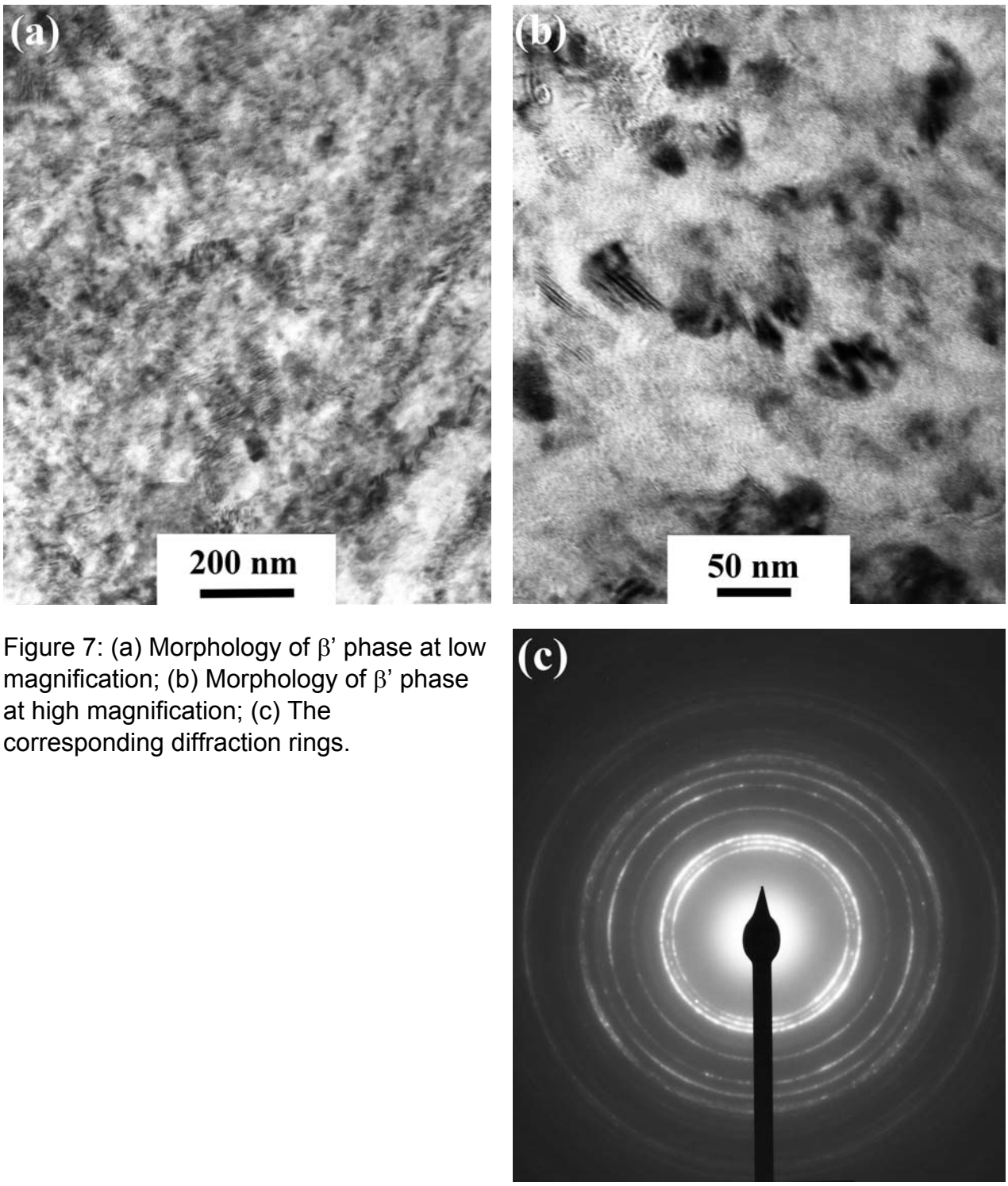

Figure 7: (a) Morphology of β' phase at low magnification; (b) Morphology of β' phase at high magnification; (c) The corresponding diffraction rings.

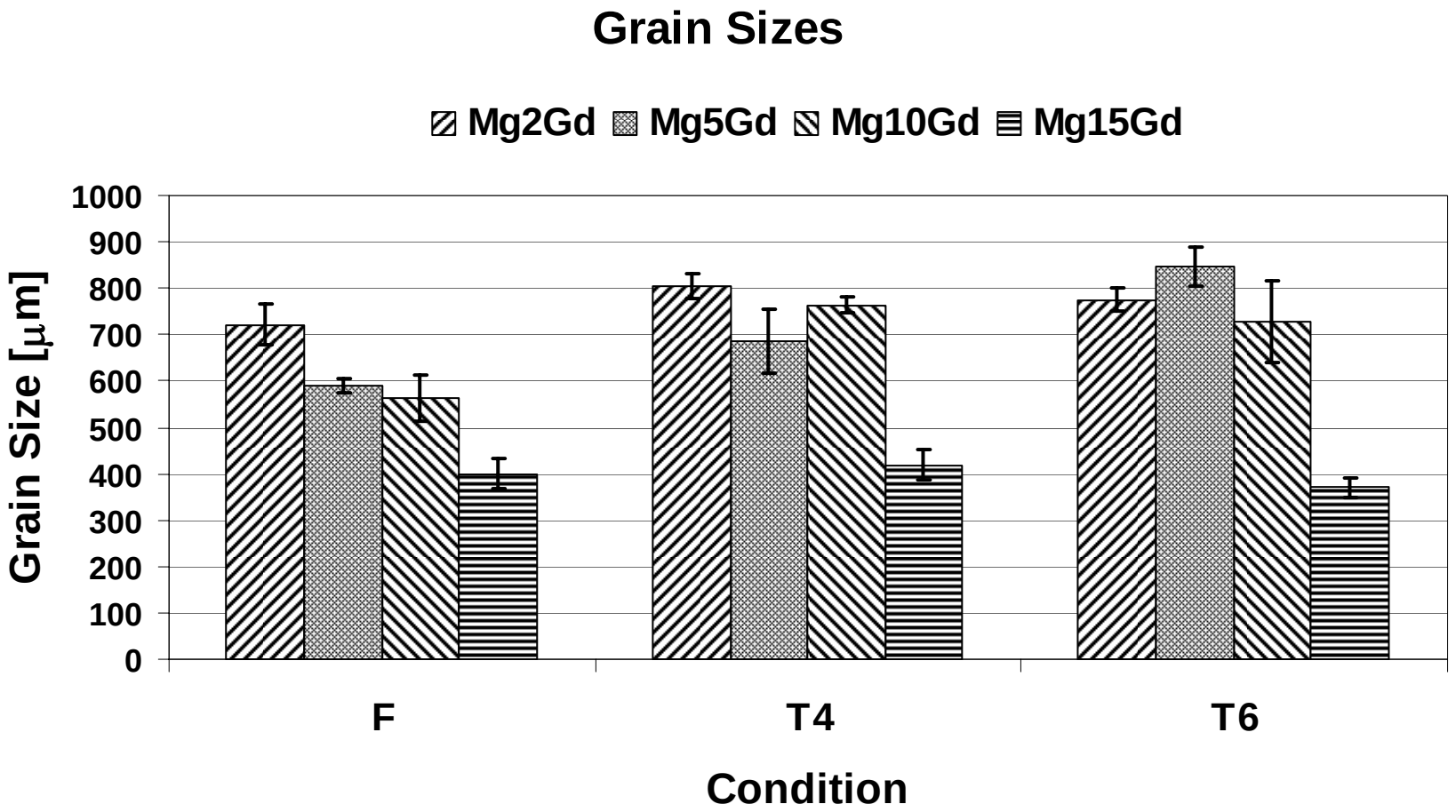

Figure 8: Grain sizes of the Mg-Gd alloys in the different heat treated conditions

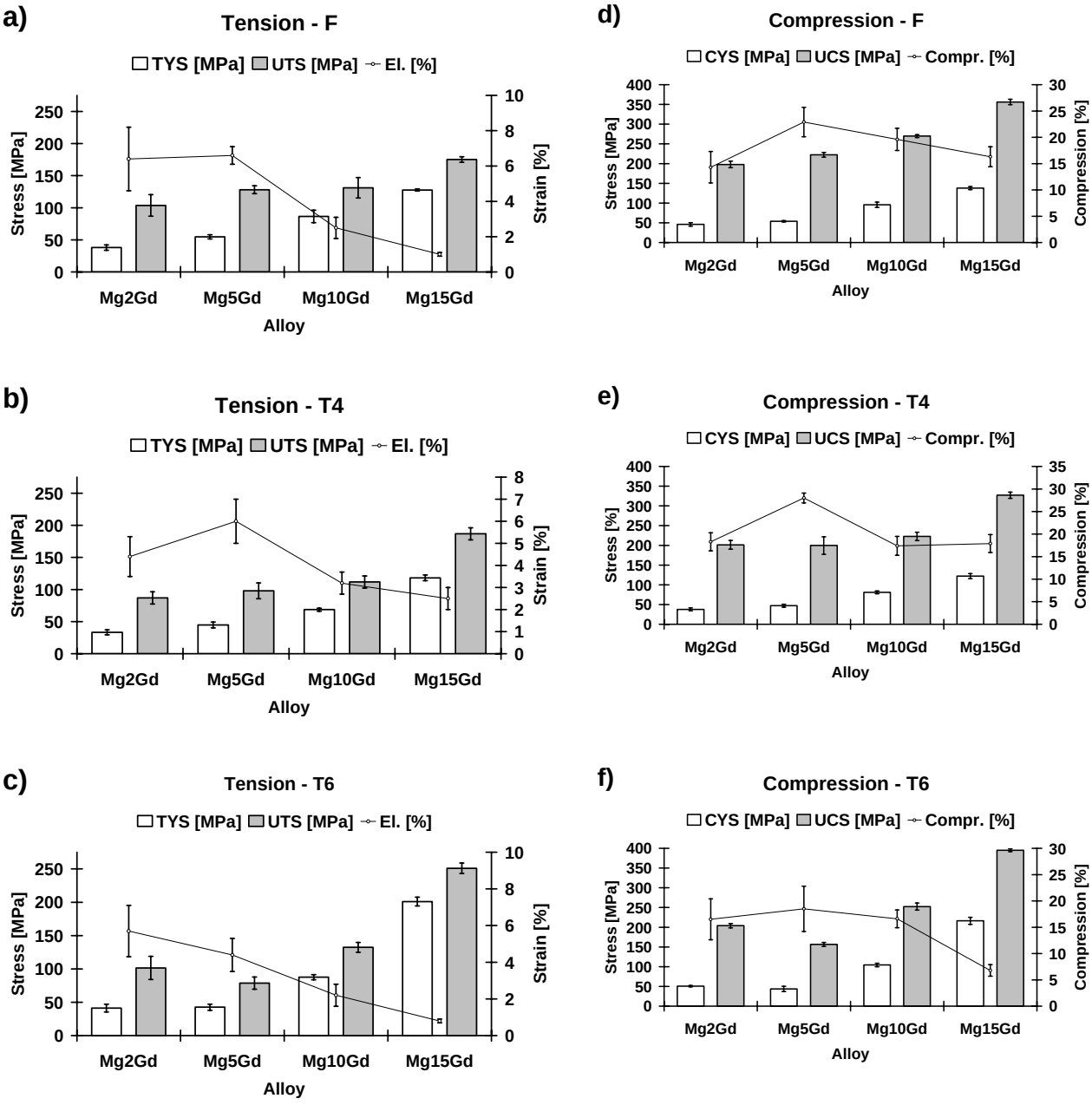

Figure 9: Mechanical Properties of the Mg-Gd alloys in tension a) F, b) T4, c) T6 and in compression d) F, e) T4, f) T6

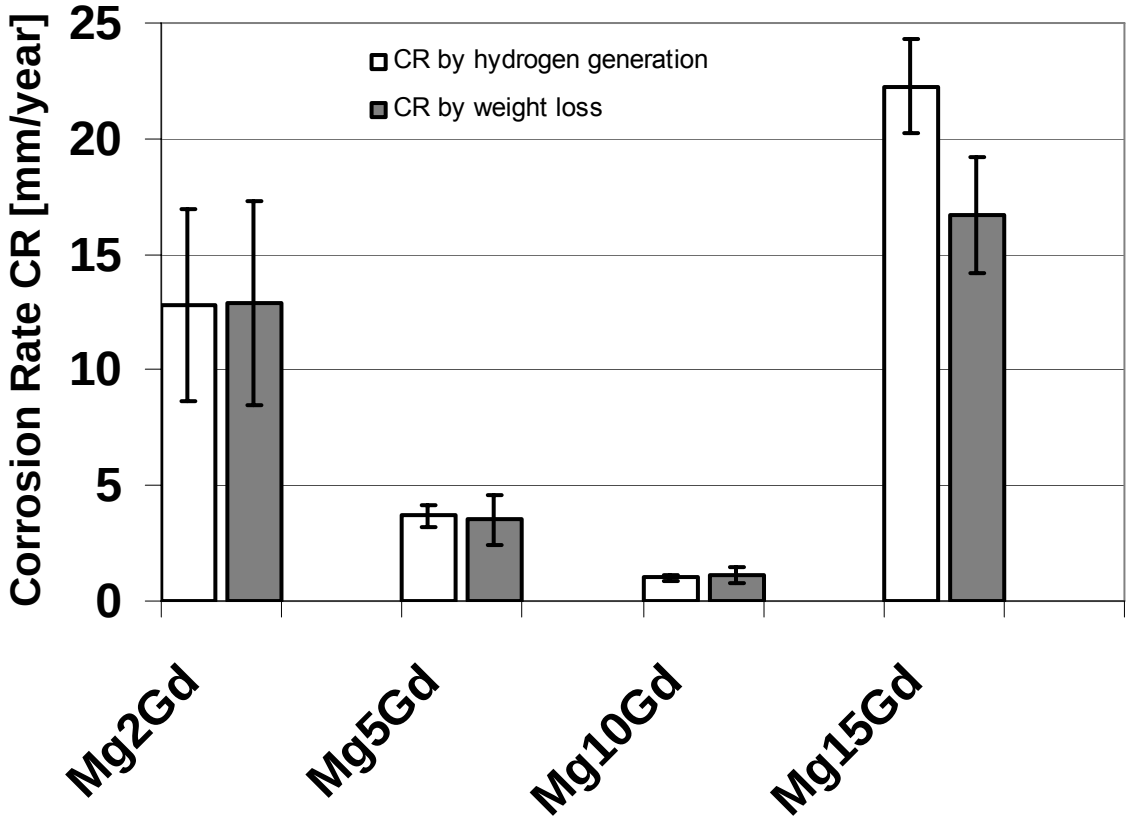

Figure 10: Corrosion rates determined by hydrogen generation and weight loss measurements